High-Temperature Water Effects on the Fracture Behaviour of Low-Alloy RPV Steels

Z. Que, H.P. Seifert, P. Spätig, S. Ritter, G. S. Rao
Paul Scherrer Institut, Nuclear Energy and Safety Research Department, Laboratory for Nuclear Materials, 5232 Villigen, Switzerland

Abstract: The structural integrity of the reactor pressure vessel (RPV) of light water reactors (LWR) is of utmost importance regarding the safety of operation and service lifetime. The fracture behaviour of low-alloy RPV steels with different microstructures (base metal, simulated weld coarse grain heat-affected zone) in simulated LWR environments was evaluated by elastic plastic fracture mechanics (EPFM) tests with different strain rates and by metallo- and fractographic post-test evaluations. These tests revealed some evidence of possible high-temperature water effects on the fracture behaviour and potential synergy with environmentally-assisted cracking and dynamic strain aging.

Keywords: Low Alloy Steel, Hydrogen Effect, Fracture Resistance Reduction, Simulated LWR Environments

1 Introduction

Structural integrity of the RPV of LWR is of utmost importance with regard to safety of operation and service lifetime and may be affected by different degradation processes like environmentally-assisted cracking (EAC) [1-3] or irradiation embrittlement [4], the latter being recognized as life limiting factor. Moreover, there is growing concern that hydrogen, absorbed from the high temperature water environment and corrosion reactions, may potentially reduce the toughness of the RPV steel in synergy (or competition) with other embrittlement mechanism like irradiation embrittlement, thermal ageing or dynamic strain aging (DSA) [5, 6]. The hydrogen concentration in the RPV from corrosion and dissolved hydrogen in the coolant in case of an intact cladding and under typical steady-state LWR power operation conditions is usually low (< 0.1 wppm), but increased critical hydrogen levels might be reached in the process zone in case of cracks in the RPV with stressed and plastically strained bare crack-tips with an aggressive occluded crack crevice chemistry and a high hydrostatic tri-axial stress state, e.g., in fracture mechanics tests in high-temperature water or in a loss of coolant accident under suitable strain rate conditions [7].

The fracture behaviour of RPV steels in high-temperature water is affected by material (strength, chemical composition, microstructure, …), environmental (temperature, chemistry of the high-temperature water, hydrogen content, …) and mechanical loading parameters (strain rate, constraints, …). There are only very few investigations on high-temperature water (HTW) and hydrogen effects on the fracture behaviour of low-alloy RPV steels in the LWR operating temperature range, since hydrogen effects usually are believed to be absent or negligible under these conditions, but they clearly indicated a potential concern and need for further more systematic investigations. Schellenberger et al. observed that the J–R curves of RPV steels were significantly lower in oxygenated high temperature water than in air and the reduction was increasing with decreasing strain rate and increasing steel sulfur content [7]. Due to the slow strain rate in these tests, the apparent toughness reduction might have been primarily caused by sub-critical strain-induced corrosion cracking. Šplíchal et al. ob-

served a severe reduction of fracture toughness in RPV steels after hydrogen charging at hydrogen contents in the steel above 1 to 2 ppm [8]. In a further study, a change of tensile properties and embrittlement of base metal and heat affected zone (HAZ) of RPV steels have been reported at certain hydrogen concentrations (2.5-3.5 ppm) [9]. Furthermore, some hydrogen effects on the EAC behaviour of low-alloy steels (LAS) in HTW [10] and synergistic effects with DSA [10, 11] were observed.

The goal of this ongoing work at Paul Scherrer Institut (PSI) is to systematically study the potential effects of high-temperature water on the fracture behavior in RPV steels and the present paper is a brief summary of the first preliminary results.

2 Materials and experimental procedure

2.1 Materials and specimens

EPFM tests according to ASTM E1820 were conducted with air fatigue pre-cracked ($a_0/W \sim 0.5$) and side-grooved (a thickness reduction of 10% on each side) 25 or 12.5 mm thick compact tension C(T) specimens (W/B = 2, T-L orientation). The tested materials are listed in **Table 1**.

Table 1: Overview on investigated RPV steels.

Desig.	Material	Product form	Micro-structure	S [%]	$YS_{288°C}$ [MPa]	Remarks
Biblis C BM	22 NiMoCr 3 7 (= SA 508 Cl. 2)	forging	base metal	0.007	400	moderate DSA & low EAC susceptibility
Biblis C HT1	22 NiMoCr 3 7	forging	coarse grain heat-affected zone	0.007	740	high strength
277	20 MnMoNi 5 5 (= SA 508 Cl. 3)	forging	base metal	0.004	418	high DSA susceptibility

The chemical composition, microstructure, mechanical tensile properties as well as DSA and EAC susceptibility of these materials have been characterized in previous investigations by PSI [7, 10-14]. The Biblis C base metal is from the lower cylindrical shell of a PWR RPV which was not commissioned. The fracture behavior of this material in high-temperature water was characterized in [7] and is thus the reference material for this study. With this material, a simulated coarse grain heat affected zone (CG HAZ), HT1, was fabricated through a specific two steps heat treatment [7]. The prior austenite grain size, microhardness/yield stress and annealed martensite microstructure are very similar to that of the high hardness CGHAZ of the actual circumferential core girth weld of the PWR RPV [7]. The 277 material shows a higher DSA susceptibility [10, 14] than the the Biblis C base metal.

2.2 Elastic plastic fracture mechanics tests

EPFM tests in both air and HTW environments at 288 and 250 °C were typically performed with a crack opening displacement rates at load line ($dCOD_{LL}/dt$) of 0.25 to 0.35 mm/min. Crack initiation and growth were monitored by the reversed direct current potential drop (DCPD) technique and the detail evaluation procedure is described in [7]. Additionally, the loading rate was varied between $3 \cdot 10^{-4}$ to 3 mm/min. J integral values at initiation of stable crack growth were calculated as per the ASTM standard (J_Q) and at “physical initiation” (J_{DCPD}). J_Q is the J value corresponding to the point of intersection between the regression line ($J = C_1 \cdot \Delta a^{C2}$) and the 0.2 mm

exclusion line. J_{DCPD} is calculated at the instant when the linear slope of DCPD potential drop vs. COD_{LL} curve starts to change and corresponds to a crack advance of ≤ ~ 50 μm [7]. The J_{DCPD} values were thus usually ~ 35 % (25 to 50 %) smaller than the corresponding J_Q values, which relate to a crack advance of ~ 200 μm. Additionally, the J integral at a crack advance of 2.5 mm (0.1 inch) $J_{0.1}$ was measured ("tearing resistance").

The EPFM tests in HTW were conducted in refreshed autoclave systems with integrated electro-mechanical loading devices that were attached to HTW loops [7, 11-13]. The corresponding tests in air were also performed in the same autoclaves. Reducing BWR hydrogen water chemistry (HWC) was simulated by hydrogenated (dissolved hydrogen (DH) content of 1.4 ppm) neutral high purity water ($pH_{288°C}$= 5.7, inlet conductivity = 0.055 $\mu S \cdot cm^{-1}$). The corresponding electrochemical corrosion potentials (ECP) of the specimens at 288 °C were -590 mV_{SHE} (HWC). PWR primary water was simulated by mildly alkaline borated and lithiated, hydrogenated high-purity water (1000 ppm B as H_3BO_3, 2.3 ppm Li as LiOH, $pH_{288\ °C}$= 6.9, inlet conductivity of 24 $\mu S \cdot cm^{-1}$, DH content of 1.8 to 1.9 ppm). The corresponding ECP at 288 °C was -735 mV_{SHE}. Selected additional tests were performed in nitrogenated (oxygen- and hydrogen-free, -400 mV_{SHE})) or oxygenated (2 ppm dissolved oxygen (DO), +100 mV_{SHE}) neutral high purity water or in PWR environment with in-situ galvanostatic hydrogen charging [7].

3 Results and discussion

3.1 As received Biblis C base metal material

Comparison of initiation toughness for the Biblis C base metal specimens tested in HTW and air at 288 °C at a loading rate of 0.25 to 0.35 mm/min for various water chemistry and test conditions are shown in **Figure 1**. For the test conditions used in this study, the HTW did not reduce the initiation toughness and tearing resistance significantly as compared to corresponding air tests and only stable ductile crack growth was observed [7]. The toughness at initiation of stable crack growth was similar for oxygenated and hydrogenated high-purity and hydrogenated moderately alkaline HTW. Duration of exposure or loading conditions during pre-oxidation in HTW did not affect the initiation toughness significantly. Additional continuous in-situ hydrogen charging under PWR conditions did not reduce the toughness (although this might not be very efficient due to the high electrolyte resistance).

However, a distinct change in fracture morphology and deformation structure [7] was observed, which was very similar to that after EPFM and tensile tests in air in the hydrogen pre-charged condition [7, 10]. Pure ductile fracture by microvoid coalescence with very limited occurrence of macrovoids was observed in air tests without hydrogen charging. The macrovoids are in most cases associated with inclusions as these are preferential sites for void nucleation. **Figure 2** shows the fracture surface of a 0.5 T-C(T) specimen after fracture toughness test in air at 288 °C without hydrogen charging. **Figure 3** (a) and (b) show typical fracture surfaces in BWR/HWC and PWR environment, respectively. Various features in addition to ductile dimples can be seen, such as macrovoids (A, **Figure 3** (a) and (b)), secondary cracks (B in **Figure 3** (b)) and quasi-cleavage facets (C, **Figure 3** (a) and (b)). Quasi-cleavage facets at inclusions were observed in some experiments, while macrovoids, secondary cracks (some of them with intergranular appearance) and flat featureless regions resembling quasi-cleavage facets, were observed after all tests in HTW. Tests in BWR and PWR

simulated conditions resulted in higher roughness of the fracture surface than corresponding experiments in air due to significantly higher macrovoid and secondary crack formation. Thus, the change in fracture and deformation mode in HTW did not significantly affect the fracture toughness and the tearing resistance at 288 °C in the as-received Biblis C base metal for the test parameters used in this study.

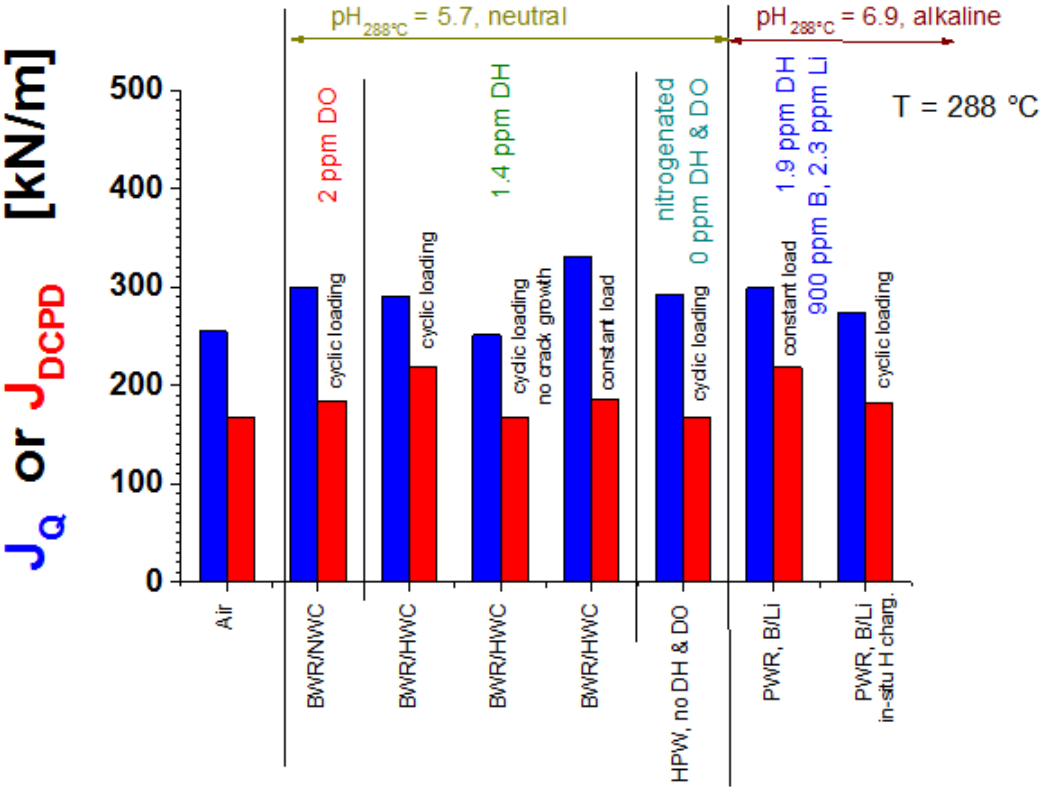

Figure 1: Comparison of J_Q and J_{DCPD} values of Biblis C base metal specimens at 288 °C in air and different HTW environments at a crack opening displacement rate of 0.25 to 0.35 mm/min.

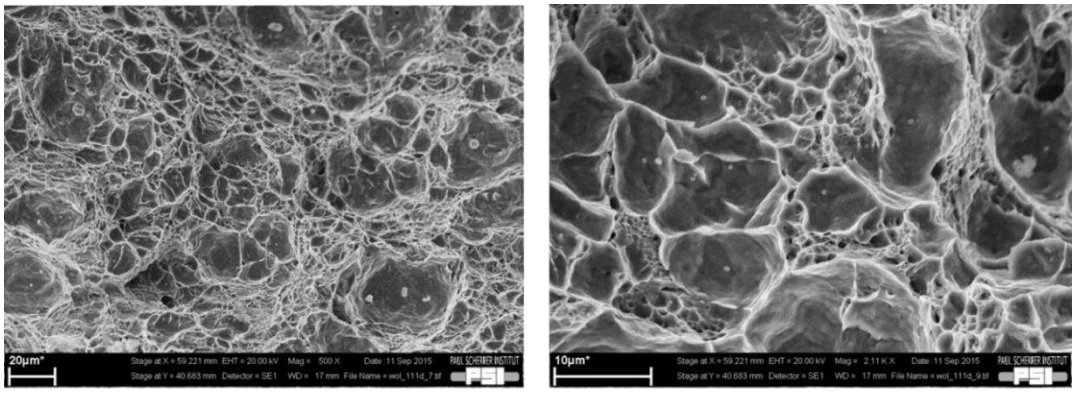

(a) (b)

Figure 2: Fractograph after fracture toughness test in air at 288 °C without hydrogen charging.

Although the EPFM tests with Biblis C base metal in HTW did not reveal significant HTW effects so far, the clear change in fracture morphology demonstrates the need for further investigations over a broader range of test conditions.

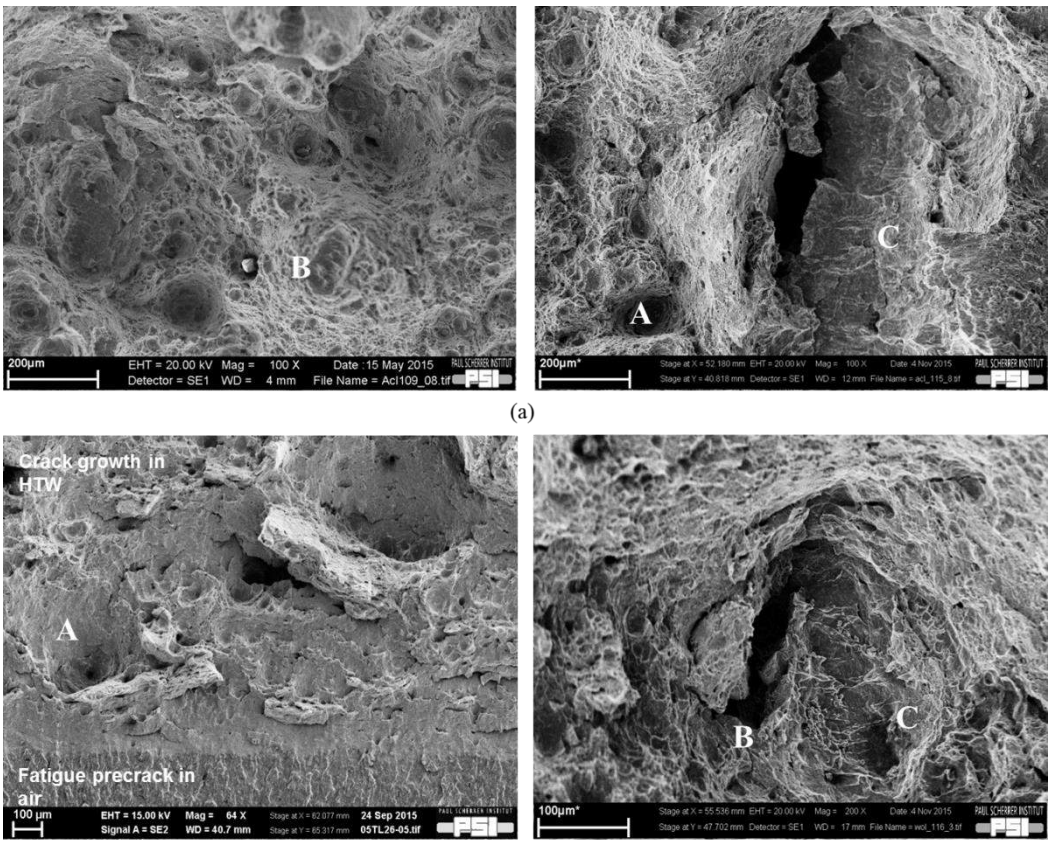

(a)

(b)

Figure 3: (a) Fracture surface of 1T-C(T) specimen in BWR showing macrovoids (A), quasi cleavage fracture (B) and localised flat quasi-cleavage facets (C); (b) fracture surface of 0.5T-C(T) specimen in PWR showing macrovoids (A), secondary cracks (B) and quasi-cleavage (C).

3.2 Simulated coarse grain heat affected zone of Biblis C material

First screening EPFM tests with the simulated high strength CGHAZ material (HT1) in hydrogenated HTW and air showed significant unstable rapid crack extensions after reaching the peak load in 0.5 and 1T C(T) specimens. Sudden instantaneous unstable crack extensions occurred after some stable ductile crack extension and beyond the peak load only. **Figure 4** (a) shows an example of unstable crack extension in the CGHAZ material and the fracture surface showed the crack growth to be predominantly ductile and there was no fractographic indication for macroscopic brittle cracking or sudden failure of large un-cracked ligaments (**Figure 4** (b)).

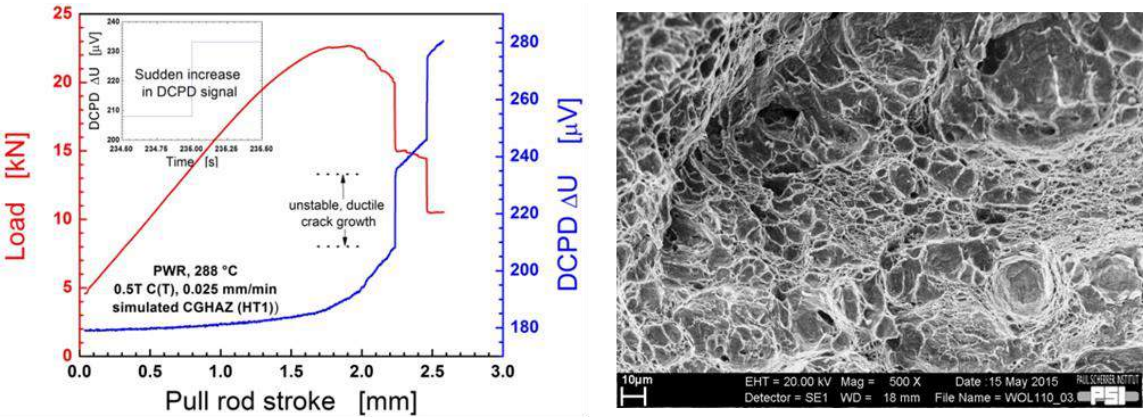

(a) (b)

Figure 4: (a) Unstable crack extension in CGHAZ material (HT1) during EPFM test in PWR HTW at a loading rate of 0.025 mm·min^{-1} and (b) corresponding fractograph showing ductile crack growth.

The unstable ductile cracking was not observed in the corresponding base metal in spite of the lower yield stress (and higher peak load to plastic limit load ratios) and might be related to plastic collapse due to low-temperature creep, DSA and strain localization, occurring simultaneously at the test temperature. Further experiments are needed and are currently in progress to show the role of HTW in the occurrences of such rapid unstable crack extensions including bigger specimens to discriminate size effects due to plastic collapse.

In contrast to the base metal, the EPFM tests in HTW with simulated CGHAZ material (HT1) indicate a potential reduction of the initiation fracture toughness and tearing resistance as well as of the J value at the onset of unstable cracking at slow loading rates ≤ 0.25 mm/min with respect to corresponding tests in air as shown in **Figure 5**. There were no indications of sub-critical EAC crack growth at the slow loading rates and crack growth was ductile in all cases. Since material scatter is significantly higher in the CGHAZ material, further tests are necessary to statistically verify this preliminary observation. Furthermore, the initiation toughness was similar in the 0.5T and 1T C(T) specimens suggesting only a weak size effect.

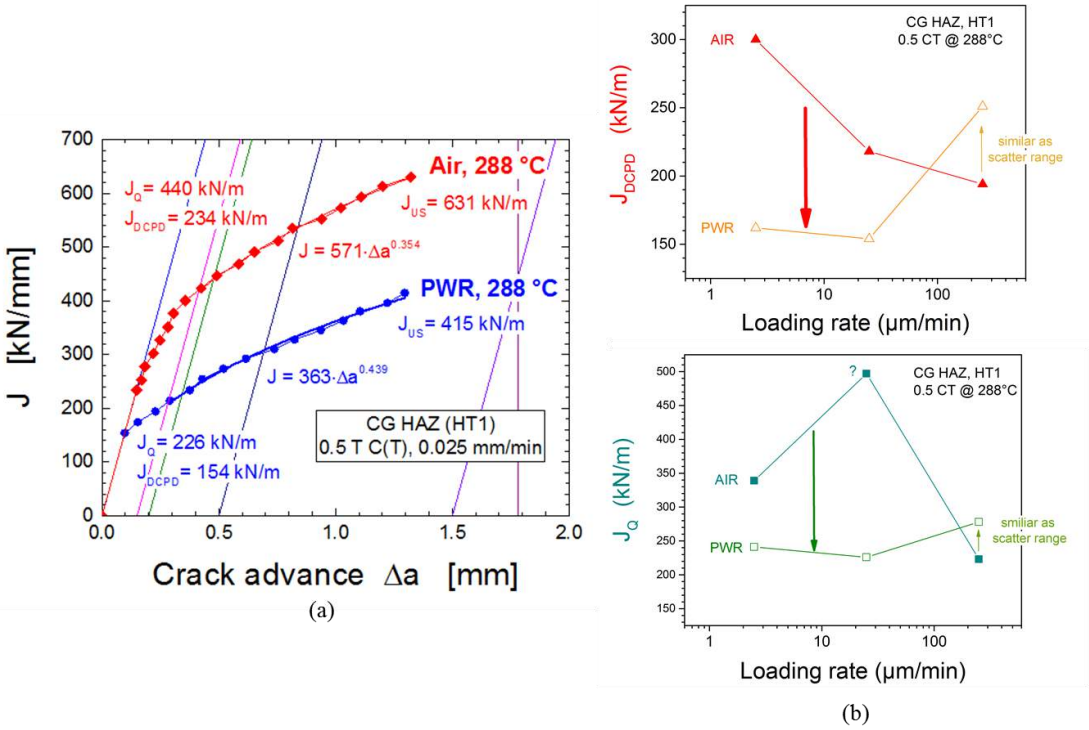

Figure 5: (a) reduction of fracture resistance of HT1 specimens at 288 °C in high-temperature water compared to test in air; (b) comparison of J_Q and J_{DCPD} values of HT1 specimens at 288 °C in high-temperature water and air environment.

The high yield stress in the CG HAZ leads to smaller crack-tip process zone size and reduction of diffusion distance, promoting hydrogen supersaturation in the process zone in front of the crack-tip due to the high tri-axial hydrostatic stress and dilatation strains. This may explain the potential higher sensitivity to HTW and hydrogen effects of the CGHAZ material [7]. The peak stress under plane strain conditions in this zone is roughly 3 times the yield stress, which results in significant low-temperature creep in the process zone due to its strong stress dependence ($d\varepsilon/dt \propto \sigma^n$). If the plastic zone is highly constrained and small enough, the logarithmic low-temperature creep ($\varepsilon \propto \log t$) usually quickly saturates and stops. With decreasing specimen size, increasing plastic zone size and load level, this situation can change. In extreme cases, the creep zone can stretch over the whole specimen due to low-temperature

creep induced stress redistributions, which could be further amplified by hydrogen enrichment and strain localization due to DSA and vice versa. The time-dependent material behavior of CGHAZ (more pronounced at slow strain rates) will be verified by constant load tests with pre-cracked specimens in air and HTW later.

3.3 277 base material with high DSA susceptibility

Tensile tests with hydrogen pre-charged 277 base materials clearly revealed that the range and amplitude of hydrogen effects are significantly amplified in the DSA temperature-strain range, suggesting synergies between DSA and hydrogen effects, resulting from localization of plastic deformation due to DSA and the shielding effect of hydrogen [10]. Furthermore, the initiation toughness and tearing resistance may be drastically reduced in the DSA temperature-strain rate range [15]. EPFM tests of 1T C(T) 277 base metal with high DSA susceptibility were performed in hydrogenated HTW and air with loading rates of 0.35 µm/min and 3.5 mm/min at 250 °C.

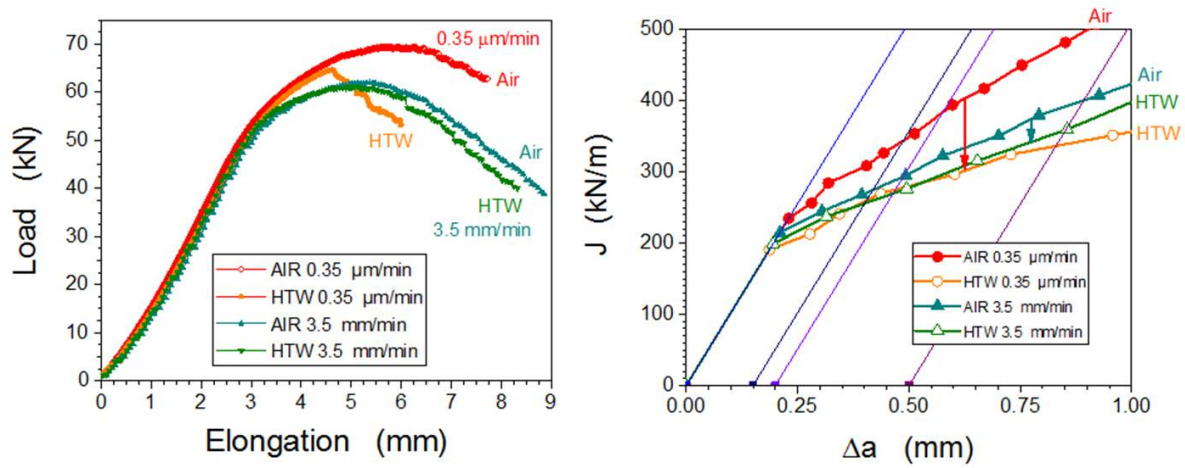

(a) (b)

Figure 6: (a) Load-displacement curve of 277 material in HTW and air at 0.35 µm/min and 3.5 mm/min; (b) Corresponding J-R curves of the EPFM tests.

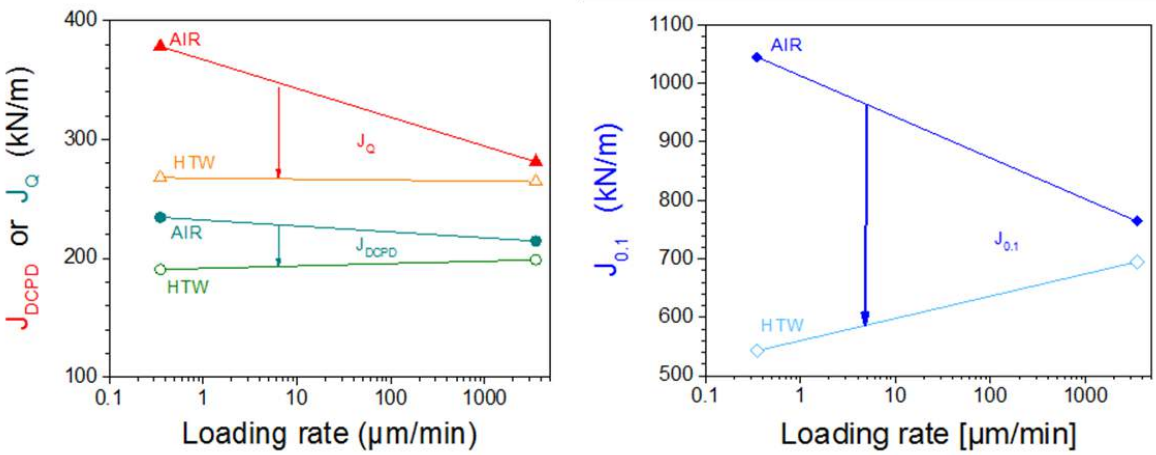

(a) (b)

Figure 7: (a) Initiation toughness of 277 material in HTW and air at 0.35 µm/min and 3.5 mm/min; (b) Corresponding tearing resistance.

Higher peak load (**Figure 6**) and initiation toughness (**Figure 7**) at lower loading rate in air was due to the negative strain rates sensitivity (increase of flow stress and ultimate tensile strength) by DSA. In hydrogenated HTW, there is a marginal and moderate reduction in initiation toughness (J_{DCPD} & J_Q) and tearing resistance ($J_{0.1}$) with decreasing loading rate, respectively (**Figure 7**). Furthermore, the HTW results in a

moderate reduction in initiation toughness and tearing resistance at fast loading rate, which becomes much more pronounced at slow loading rate (**Figure 7**). Tests in air and at the fast loading rate in HTW, the fracture was fully ductile by microvoid coalescence. In contrast, the fracture mode at slow loading rate in HTW was significantly different (**Figure 8**). Here the crack first initiated in a stable ductile mode by microvoid coalescence but then propagated by sub-critical strain-induced corrosion cracking (SICC) with “high-sulphur” EAC crack growth rate [1, 12, 13, 16] at higher J levels. The strong apparent reduction in tearing resistance at the slow loading rate is thus mainly related to SICC crack growth. In the COD curve of **Figure 6** (a), several small unloadings could be seen, e.g., at the end of the test arising from fast local crack growth (failure of large un-cracked ligaments, large steps between the individual fan-shaped SICC cracks). These unloadings can result in a temporary decrease of J and stop of SICC crack growth. Then crack growth has first to re-initiate by microvoid coalescence, when J is increasing again, as it was the case in this test.

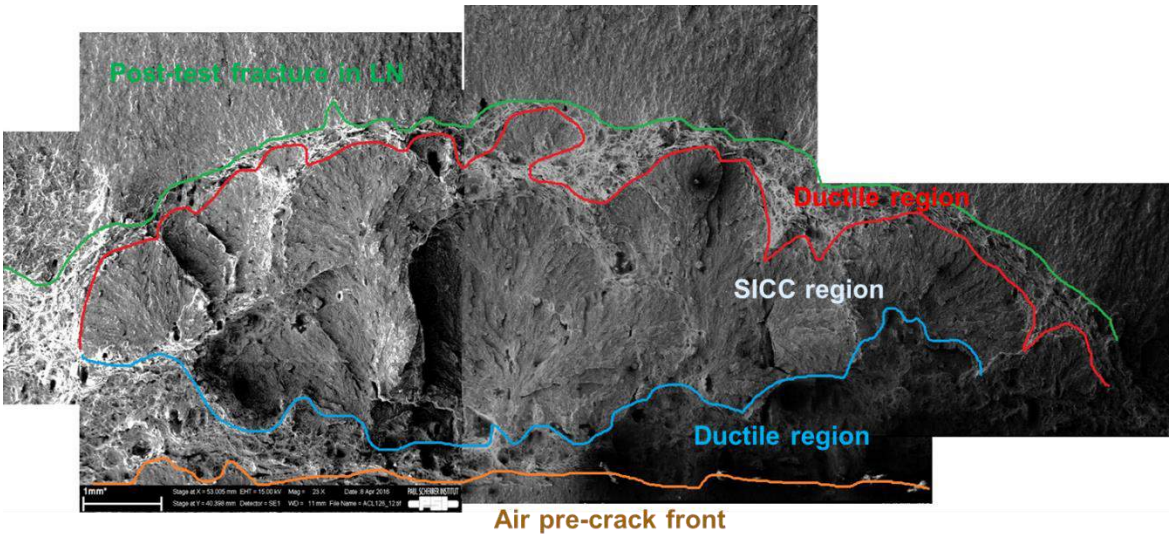

Figure 8: Fracture surface of 277 steel in EPFM test at 0.35 µm/min in HTW at 250 °C.

The SICC crack growth rate and fractographic appearance was identical to those in slow rising load tests at the same loading rate in oxygenated HTW [12], but SICC initiated at much higher K_I values (> 200 vs. 35 MPam$^{1/2}$), as indicated in **Figure 9**. The SICC crack growth rate for the test with a loading rate of 0.35 µm/min in HTW ($1.3 \cdot 10^{-8}$ m/s) was a factor of ~2.4 higher than the ductile crack growth rate in air ($5.3 \cdot 10^{-9}$ m/s). The ductile crack growth rate at a loading rate of 3.5 mm/min, on the other hand, was about $8 \cdot 10^{-5}$ m/s for both tests in HTW and air and significantly faster than the maximum EAC rates by dissolution of $3 \cdot 10^{-7}$ m/s. Here the resulting crack-tip strain rate of 10^{-2} s^{-1} is too high for EAC crack growth [1]. EAC crack growth in LAS in HTW is a superposition of the film rupture/anodic dissolution mechanism and hydrogen-assisted EAC mechanism, whereas dissolution seems to dominate the crack advance in case of SICC crack growth [1, 12]. DSA is more pronounced at the slower strain rate and results in plastic deformation localization due to the negative strain rate sensitivity. These localized deformation bands are preferred regions for hydrogen enrichment, which further amplifies the localization of plastic deformation by hydrogen (HELP mechanism) [7, 10] with positive feedback effects. The localization of plastic deformation also favors rupture of the protecting oxide film, subsequent anodic dissolution and further hydrogen uptake and thus may explain the presence of SICC in the 277 steel with high DSA susceptibility, but its absence in the Biblis C base metal under otherwise identical conditions.

The EAC crack growth rate is dependent on crack-tip strain rate, which in turn is dependent on loading rate dk/dt (dJ/dt) and crack growth rate da/dt (and K or J) in SSRT tests. Both crack-tip strain rate and crack-crevice chemistry depend on crack growth rate and vice versa in LAS in HTW with positive feedback effects [1] and a dynamic equilibrium can be established. The crack crevice chemistry is more aggressive in case of oxygenated HTW (sulphur-anion enrichment due to potential gradient), but aggressive high-sulphur crevice conditions can also be achieved at low ECP by the exposure and dissolution of new fresh MnS-inclusions and the slow transport of the sulphur-anions out of the crack by diffusion, if the crack is growing with a sufficiently fast rate. A significantly higher K or J is necessary to achieve this situation at low ECP without sulphur-anion enrichment by the anion pump and the same EAC crack growth rates are observed for the same crack-tip strain rates. Besides this EPFM test, fast "high-sulphur" EAC was observed in high-purity water at low ECP in cyclic load tests [13], if loading frequency was high and crack growth fast enough. Probably, some prior ductile crack growth is necessary to establish this dynamic equilibrium in a SSRT test. These preliminary results indicate potential synergies of hydrogen/HTW embrittlement with EAC and DSA under suitable system conditions and suggest a continuous spectrum between EAC and HTW/hydrogen effects on fracture, which clearly asks for further systematic studies.

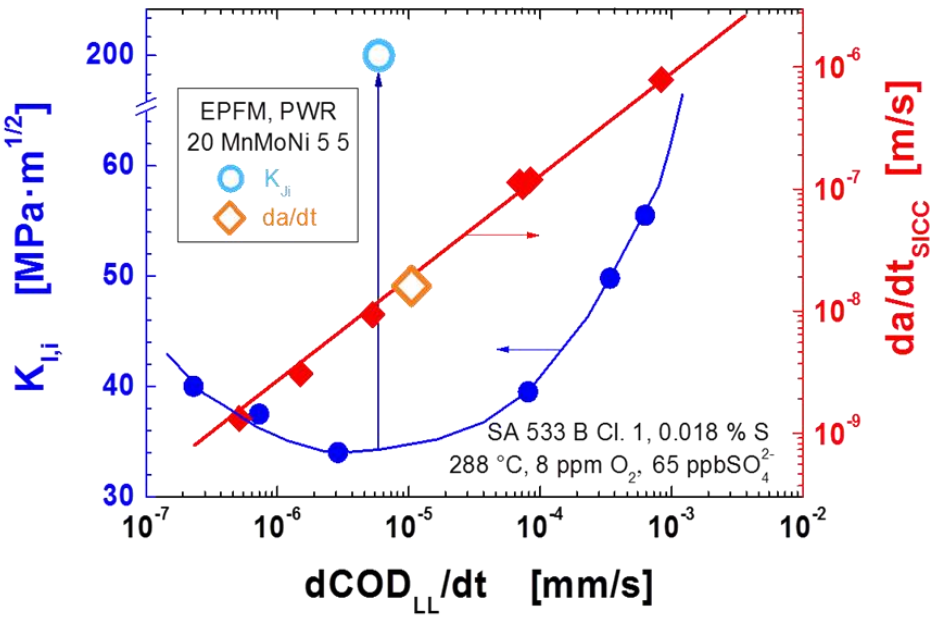

Figure 9: Comparison of SICC crack growth rate and initiation toughness K_{IJ} of 277 steel in hydrogenated HTW in an EPFM test at 0.35 µm/min with corresponding rates and stress intensity factors $K_{I,i}$ at initiation of SICC in oxygenated HTW in slow rising load EAC tests.

4 Summary, conclusions and outlook

The fracture behaviour of RPV low alloy steels in simulated LWR environments was evaluated by EPFM tests with different strain rates and by fractographic post-test evaluations. Exposure to HTW (PWR, BWR/NWC, BWR/HWC) of Biblis C base metal material at 288 °C did not reduce the initiation toughness and tearing resistance, although a clear change in fracture morphology was observed. In the simulated CG HAZ material, occurrences of sudden unstable ductile crack extensions and evidence for possible reduction of the initiation toughness in hydrogenated HTW was observed, but further tests are needed. First tests with the 277 steel with high DSA susceptibility revealed clear evidence for initiation toughness and tearing resistance re-

duction in hydrogenated HTW due to the synergy between DSA and HTW/hydrogen effects, but results at slow loading rate were affected by SICC crack growth.

Further EPFM tests with systematic variation of environmental, material and loading parameters and detailed post-test characterization by TEM, SEM and EBSD are planned, followed by the FEM modeling of local crack-tip stress/strain fields and local approaches to fracture to better understand the underlying mechanism. More pronounced effects on fracture resistance reduction can be expected with more susceptible materials (high sulphur steels with high EAC susceptibility, CGHAZ with high yield stress, steels with high DSA susceptibility), at lower temperatures (with stronger hydrogen-deformation effects) or under suitable critical loading/strain rate conditions.

5 Acknowledgment

Funding for the SAFE-II project from the Swiss Federal Nuclear Safety Inspectorate (ENSI) is gratefully acknowledged. The authors would like to express their gratitude for the experimental contributions of D. Stammbach, B. Baumgartner, R. Schwenold and H. Kottmann from Paul Scherrer Institut.

6 References

[1] H.P. Seifert, J. Hickling, and D. Lister, Corrosion and environmentally-assisted cracking of carbon and low-alloy steels, in: Comprehensive Nuclear Materials, Editor R.J.M. Konings, Elsevier: Oxford, UK, ISBN: 978-0-08-056033-5, pp. 105-142, 2012.

[2] J. Hickling, D. Blind, Nucl Eng Des 91 (1986) 305-330.

[3] H. Seifert, J Nucl Mater, 378 (2008) 312-326.

[4] N. Soneda, Irradiation Embrittlement of Reactor Pressure Vessels (RPVs) in Nulcear Power Plants, Woodhead Publishing Series in Energy: Number 26, Woodhead Publishing, Cambridge, UK, 2015.

[5] P. L. Andresen, Corrosion, 64 (2008) 439-464.

[6] S. Roychowdhury et al., Effect of high-temperature water and hydrogen on the fracture behaviour of a low-alloy reactor pressure vessel steel, 17th Int. Conference on Environmental Degradation of Materials in Nuclear Systems - Water Reactors, Ottawa, Canada, 2015.

[7] S. Roychowdhury et al., Effect of high-temperature water and hydrogen on the fracture behavior of a low-alloy reactor pressure vessel steel, accepted for publication in J Nucl Mater, 2016.

[8] K. Šplíchal et al., Int J Press Ves Pip, 55 (1993) 361-373.

[9] S. Kim, Metall. Mater. Trans A, 31 (2000) 1107-1119.

[10] G. S. Rao et al., Effect of hydrogen on tensile behavior of low alloy steel in the regime of dynamic strain ageing, 21st European Conference on Fracture, ECF21, 20-24 June 2016, Catania, Italy, to be published in Structural Integrity Proceedia.

[11] H.P. Seifert, S. Ritter, J of Nucl Mater 372 (2008) 114 – 131.

[12] H.P. Seifert, S. Ritter, J of Nucl Mater 378 (2008) 312 – 326.

[13] H.P. Seifert, S. Ritter, Corr Sci 50 (2008) 1884 – 1899.

[14] H. Hänninen, H.P. Seifert, Y. Yagodzinsky, U. Ehrnstén, O. Tarasenko, P. Aaltonen, Effects of dynamic strain ageing on environment-assisted cracking of low alloy pressure vessel and piping steels, in: 10th Int. Conf. on Environmental Degradation of Materials in Nuclear Power Systems – Water Reactors, NACE/TMS/ANS, Lake Tahoe, Nevada, USA, August 6 - 10, 2001.

[15] J J.H Yoon, B.S Lee, Y.J Oh, Int J Press Ves Pip, 76 (1999) 663-670.

[16] F.P. Ford, J Pres Ves Technol, 110 (1988) 113-128.